A Three-Dimensional Parallel Radiative Transfer Model for Atmospheric Heating Rates for use in Cloud Resolving Models — the **TenStream** solver

Fabian Jakub*, Bernhard Mayer

Ludwig-Maximilians Universität München

Abstract

This paper presents a new method to compute three-dimensional heating rates in atmospheric models, in particular numerical weather prediction models and large eddy simulations. The radiative transfer in such models is usually calculated for each vertical column independently of its neighbouring columns. Earlier studies showed that the neglect of horizontal energy transport introduces significant errors at model grid spacings below 1 km. To date, there is no method to calculate 3D heating rates which is fast enough to systematically study the effect of radiation on cloud evolution. Here, we present a new algorithm which provides a fast yet accurate approximation for realistic three-dimensional heating rates. The method extends the well-known one-dimensional TwoStream theory to ten streams in three dimensions. Special emphasis is laid on scalable parallelism and speed.

It is found that the new solver significantly reduces the root mean square error for atmospheric heating and surface heating rates when compared to traditionally employed one-dimensional solvers. The TenStream solver reduces the relative root mean square error of heating rates by a factor of five when compared to the independent column approximation. In the case of a strato-cumulus cloud field and the solar zenith angle being 60°, the error was reduced from 171% to 31% and for a deep-convective cumulus cloud from 158% to 30%. The model described here will open the way to answer the question, if and how much three-dimensional radiative transfer effects indeed affect cloud development and precipitation.

Keywords: 3D, Radiation, Heating Rate, LES, NWP, Parallel

1. Introduction

The next generation of numerical weather prediction (NWP) models shift from statistical cloud parametrizations to physics based convection schemes by increasing the horizontal resolution to considerably less than 1km. This shift also necessitates the correct treatment of solar and thermal radiative transfer (RT). Recent studies (Frame et al., 2009; O'Hirok and Gautier, 2005) showed that three-dimensional RT – currently neglected by all atmospheric models because of the associated high computational cost – may have considerable impact on cloud formation and precipitation. Realistic three dimensional heating rates may also prove essential for the correct representation of droplet micro-physics and the corresponding vapour growth rates (Harrington et al., 2000; Marquis and Harrington, 2005). It remains to be shown if 3D RT causes changes beyond increasing small-scale variability and if currently employed 1D RT operators should be replaced by computationally more expensive 3D solvers.

O'Hirok and Gautier (2005); Wapler and Mayer (2008); Wissmeier et al. (2013) found that using the independent column approximation (ICA) for horizontal resolutions below 1 km introduces significant errors in surface irradiance and atmospheric heating rates. The ICA calculates radiation for each column independently of each of its neighbouring columns, thus neglecting any horizontal energy transport. Neither cloud side illumination nor the

*Corresponding author

Email address: fabian@jakub.com (Fabian Jakub)

fact that cloud shadows are shifted are considered in one-dimensional calculations.

Currently available 3D RT solvers (Monte Carlo based (e.g. Mayer (2009)) or SHDOM (Evans, 1998)) are cumbersome to use because of their extraordinary computational burden. In the past, the RT community employed two approximations to account for 3D effects, namely the tilted independent column approximation (TICA – sometimes called "tilted independent pixel approximation", TIPA) as well as the non-local independent column approximation (NICA). In the TICA, the direct solar radiation is calculated along a tilted coordinate system. The NICA accounts for horizontal energy diffusion by smoothing the irradiance field over several columns. An overview of these two approximations is given by Wissmeier et al. (2013). While the TICA and NICA do result in greatly improved surface irradiance fields, it is not straightforward to apply these approximations to calculate atmospheric heating rates.

The purpose of this work is to develop a new, truly three-dimensional solver, which is able to compute realistic atmospheric heating rates, yet is fast enough to run in high resolution models. In Section 2 we will introduce the basic concept of a finite volume solver, in close analogy to the well established TwoStream approximation (Meador and Weaver, 1980) and expand it to 10-streams in three dimensions. The new algorithm will then be compared to a 3D Monte Carlo solver for a variety of cloud scenarios with varying horizontal resolution and meteorological situations in section 3.
Section 4 will discuss the advantages and drawbacks of the developed method and its applicability for NWP models and large eddy simulations.

2. Method

The general outline of any finite volume algorithm such as the TwoStream solver is straightforward. The first step is to solve the radiative transfer inside a single volume (horizontal layer in 1D, box in 3D). As a second step, the individual volumes have to be coupled to one another. In the following we will revisit the TwoStream formulation and note the key components. TwoStream solutions give the up- and downward fluxes $E_\uparrow$ and $E_\downarrow$ for a horizontally infinite and homogeneous layer and can be written as:

$$\begin{aligned} E_\uparrow^T &= \gamma_1 E_\uparrow^B + \gamma_2 E_\downarrow^T + \beta_0 S^T \\ E_\downarrow^B &= \gamma_2 E_\uparrow^B + \gamma_1 E_\downarrow^T + \beta_1 S^T \end{aligned} \tag{1}$$

where the superscript ^{T} and ^{B} denote the upper and lower bound of the layer.

The source term S in the solar spectral region is the direct irradiance which is calculated as follows:

$$S^B = \alpha\, S^T \tag{2}$$

α is the transmission of direct irradiance which can be expressed by Lambert-Beer's law:

$$\alpha = \exp\left(-\int k_{ext}\; ds\right) = \exp\left(-\frac{\tau}{\mu_0}\right) \tag{3}$$

where k_{ext} is the extinction coefficient, τ is the vertical optical thickness of the layer, and μ_0 the cosine of the solar zenith angle.

The individual transport coefficients in a TwoStream solver describe the following processes:

- Direct radiation (S) is the part of the radiation which has not yet interacted with the medium; its transmission is described by (α).
- Direct radiation, after scattering, is the source of diffuse radiation, either scattered into the upper (β_0) or the lower (β_1) hemisphere.
- Diffuse radiation (E) is subject to absorption and scattering. The coefficients γ_1 and γ_2 describe diffuse transmission and reflection.

The transport coefficients β and γ are obtained by solving a simplified radiative transfer equation for a homogeneous layer. E.g. the delta-Eddington approximation assumes that the radiance is a linear function of the polar angle. Here we don't look into the details of the derivation of TwoStream solutions. Interested readers may refer to Meador and Weaver (1980).
For calculations in a vertically inhomogeneous atmosphere, the atmosphere is usually split into a number of homogeneous layers. For each of those homogeneous layers, the coefficients α, β, and γ are calculated as outlined above. To obtain a solution for the inhomogeneous atmosphere, the individual layers are coupled by substituting the incoming flux at the upper or lower boundaries by the outgoing fluxes at the adjacent layers. This results in an

equation system which, considering boundary conditions at the lowermost and uppermost levels, allows for the solution of a vertically inhomogeneous atmosphere (details in section 2.4).

2.1. Concept for a new solver

Two streams only allow for energy transport along a single axis. Consequently, two are certainly not enough for a reasonable 3D approximation. Well, how many streams are needed and how many can we afford computationally? To answer this question, we developed a flexible framework for studying a variety of discretizations.

The simplest discretization for the diffuse radiation on a rectangular grid would be six streams, namely two in the vertical, as it is the case in TwoStream solvers ($E_\uparrow$,$E_\downarrow$), and additionally two streams for each horizontal direction. Additionally, direct radiation necessitates three streams, one in each direction (x,y,z), which we will denote as $S_\downarrow$, $S_\rightarrow$ and $S_\searrow$. It does, however, turn out that a single diffuse stream for each sideward direction fails to describe the 3D radiation field adequately which shows in only marginally improved results regarding atmospheric heating rates. As a consequence, this paper will use ten streams for diffuse and three streams for direct radiation. Section 3 briefly explains why we recommend the above setup for use in LES or NWP models.

Setting up the equation system to couple individual homogeneous grid boxes for a TenStream system is analogous to the TwoStream approach. However, our approach in calculating the transport coefficients differs significantly. Instead of an approximate analytic expression, we use Monte Carlo methods (Mayer, 2009) to compute the transport coefficients (see section 2.3). The advantage of the Monte Carlo method is that it does not need any simplifying assumptions and that the tedious integration of the radiative transfer equation over the grid box volume is avoided. Since Monte Carlo is computationally expensive, the coefficients are precomputed for a large set of atmospheric conditions and stored in a lookup-table (section 2.3).

2.2. Discretization of streams

This section defines the explicit discretization of the ten diffuse and three direct streams. For illustration purposes we present two dimensions and omit the third one (North-South) for reasons of clarity, which reduces the number of streams from ten to six diffuse streams and from three to two direct streams. Adding the third dimension is trivial.

In analogy to the TwoStream formalism in eq. (1), we can write the transport of incoming (right-hand side) to outgoing (left-hand side) radiation as follows:

$$\begin{bmatrix} \mathrm{E}^{\mathrm{T}}_{\uparrow} \\ E^{\mathrm{B}}_{\downarrow} \\ E^{\mathrm{L}}_{\swarrow} \\ E^{\mathrm{R}}_{\searrow} \\ E^{\mathrm{L}}_{\nwarrow} \\ E^{\mathrm{R}}_{\nearrow} \\ S^{\mathrm{B}}_{\downarrow} \\ S^{\mathrm{R}}_{\rightarrow} \end{bmatrix} = \begin{bmatrix} \gamma_1 & \gamma_2 & \gamma_3 & \gamma_3 & \gamma_4 & \gamma_4 & \boldsymbol{\beta}_{01} & \boldsymbol{\beta}_{11} \\ \gamma_2 & \gamma_1 & \gamma_4 & \gamma_4 & \gamma_3 & \gamma_3 & \boldsymbol{\beta}_{02} & \boldsymbol{\beta}_{12} \\ \gamma_5 & \gamma_6 & \gamma_7 & \gamma_8 & \gamma_9 & \gamma_{10} & \boldsymbol{\beta}_{03} & \boldsymbol{\beta}_{13} \\ \gamma_5 & \gamma_6 & \gamma_8 & \gamma_7 & \gamma_{10} & \gamma_9 & \boldsymbol{\beta}_{04} & \boldsymbol{\beta}_{14} \\ \gamma_6 & \gamma_5 & \gamma_9 & \gamma_{10} & \gamma_7 & \gamma_8 & \boldsymbol{\beta}_{05} & \boldsymbol{\beta}_{15} \\ \gamma_6 & \gamma_5 & \gamma_{10} & \gamma_9 & \gamma_8 & \gamma_7 & \boldsymbol{\beta}_{06} & \boldsymbol{\beta}_{16} \\ 0 & 0 & 0 & 0 & 0 & 0 & \boldsymbol{\alpha}_{00} & \boldsymbol{\alpha}_{10} \\ 0 & 0 & 0 & 0 & 0 & 0 & \boldsymbol{\alpha}_{01} & \boldsymbol{\alpha}_{11} \end{bmatrix} \begin{bmatrix} \mathrm{E}^{\mathrm{B}}_{\uparrow} \\ E^{\mathrm{T}}_{\downarrow} \\ E^{\mathrm{R}}_{\swarrow} \\ E^{\mathrm{L}}_{\searrow} \\ E^{\mathrm{R}}_{\nwarrow} \\ E^{\mathrm{L}}_{\nearrow} \\ S^{\mathrm{T}}_{\downarrow} \\ S^{\mathrm{L}}_{\rightarrow} \end{bmatrix} \tag{4}$$

The lower two rows of eq. (4), i.e. the α-coefficients, specify the transport of direct radiation through the box (see eq. (2) for reference to the TwoStream formalism).
As fig. 1a shows, $\mathrm{S}^{\mathrm{T}}_{\downarrow}$ is the incoming solar radiation through the top of the box and $\mathrm{S}^{\mathrm{L}}_{\rightarrow}$ through the side wall. For direct radiation the superscripts ^{L} and ^{R} are chosen for the sun shining from the left. If the sun is positioned on the opposite side, they may be switched. The α-coefficients are still calculated by Lambert-Beer's Law but the integral in eq. (2) is not a constant expression anymore. It rather has to be integrated over all possible paths a photon can travel through the box. Some coefficients may be zero, depending on the geometry. For example, α_{11} is zero unless the solar zenith angle is so high that direct radiation may enter at the left side and exit the box on the right.

The diffuse streams $E_\uparrow$ and $E_\downarrow$ are analogous to the TwoStream formulation defined as the flux through the top and bottom of the box. Figure 1b also shows the two streams on each side wall, where $E_\searrow$ is the flux through the side wall into the lower hemisphere, whereas $E_\nearrow$ corresponds to the upper hemisphere. In the vertical, the superscripts ^{T} and ^{B} again denote the top and bottom of the box. In the horizontal direction, the left side is denoted with superscript ^{L} and the right side with ^{R}. The β-coefficients describe the conversion from direct to diffuse radiation, i.e. how direct light is scattered into one of the diffuse streams. Finally, the γ-coefficients characterize the energy transport between the various diffuse streams. Note that γ-

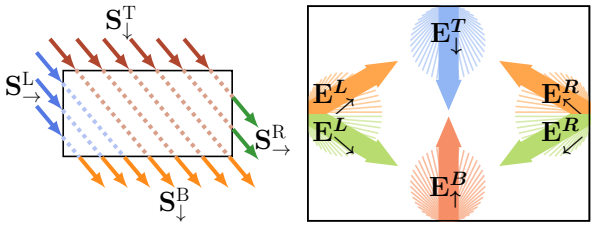

(a) direct streams (θ=40°) (b) diffuse streams

Figure 1: Discretization for three direct and ten diffuse streams (two and six in 2D respectively). Figure 1a shows incoming and outgoing direct radiation, traveling (dashed) through the box ($\boldsymbol{\alpha}$). In case that direct radiation is scattered (not depicted), radiation will be transferred to diffuse streams ($\boldsymbol{\beta}$). Figure 1b shows incoming diffuse radiation ($\boldsymbol{\gamma}$). Diffuse outgoing streams (not depicted) are identical to incoming streams but with reversed directions.

coefficients in eq. (4) occur more than once. The reason for these symmetries are streams at opposing sides which are symmetric. This is already the case in the TwoStream approximation for the up- and downward streams, and of course also holds true for sideward streams.

2.3. Calculating the Transport Coefficients

An analytic solution of a simplified radiative transfer equation, in analogy to the TwoStream method would be rather tedious, if possible at all. And even if possible, it would only be approximate. We therefore decided to use a Monte Carlo method to derive the transport coefficients (eq. (4)) which is straightforward to implement and more accurate than any analytical approximation.

The principal idea of Monte Carlo radiative transfer is to not explicitly solve the radiative transfer equation, but rather to model the underlying processes i.e. absorption and scattering. Statistical sampling of individual photon paths yields the desired solution to the radiative transfer equation, in particular the transport coefficients. The beauty of Monte Carlo methods lies in their flexibility and ease of use, which allows us to freely play around with a variety of streams. Also, there are no restrictions to geometry: triangular or hexagonal grids (as used by modern NWP models) may be implemented as easily as a rectangular grid.

For example, to calculate the direct radiation transport coefficients α_{00} and α_{01}, we have initialized photon packets uniformly distributed on the top of the box while the direction is fixed with the solar zenith and azimuth angle. After tracing a photon through the box and given that it is not scattered or absorbed, it ends up in either $S^B_\downarrow$ or $S^R_\rightarrow$ and consequently accounts for α_{00} or α_{01}. On the other hand, if the photon is scattered, it contributes to one of the diffuse streams and hence adds to a β-coefficient.

The same procedure is used for the diffuse γ-coefficients. For example, photons for the $E_\downarrow$ stream are initialized at the box top, assuming isotropic radiance that is uniformly distributed in space and the angles are chosen according to a lambertian surface.

At this point we should review the approximations just introduced. While the Monte Carlo methods are not using simplifications for the sub-grid radiative transfer, we do however limit the resolution of the radiance field spatially as well as angularly through assumptions made on the boundaries of a box. On one hand, the size of the boxes, i.e. the resolution of the grid determines the spatial resolution. On the other hand, we need to make an assumption about the angular distribution of incoming light and hence, the count and orientation of the streams define the angular resolution.

This study uses a simple forward Monte Carlo model that calculates the transport coefficients for one homogeneous box. Without looking into the details of the model, we should still briefly mention its key features. If not noted otherwise, please refer to Mayer (2009) for a detailed explanation. For cloud scattering we used the Henyey-Greenstein phase function (Henyey and Greenstein, 1941). Absorption is accounted for by reducing the photon weight. The integration is performed until the absolute standard deviation is less than 10^{-3} and the relative standard deviation is smaller than 10%. To speed up the calculation in the case of high optical thicknesses we used Russian roulette as proposed by Iwabuchi (2006).

This calculation is accurate but too slow to be run online for every box, hence we pre-computed the coefficients and saved them in a lookup table. The dimensions of the look-up table are the box size and its optical properties, namely the scattering and absorption coefficient and the asymmetry parameter of the phase function. In addition, the coefficients for the direct radiation, α and β, depend on the solar zenith and azimuth angles.

2.4. Coupling boxes and solving the matrix equation

When the energy flow is described inside each box, the next step is to couple the individual boxes. The incoming flux at the upper boundary $E^T_\downarrow$ of

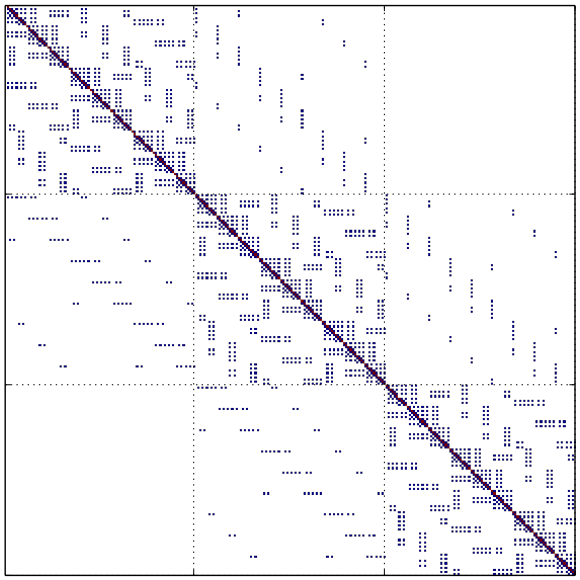

Figure 2: Nonzero pattern of a diffuse TenStream matrix with grid size being $3 \times 3 \times 3$. At a closer look, the 3 by 3 by 3 by 10 structure is evident.

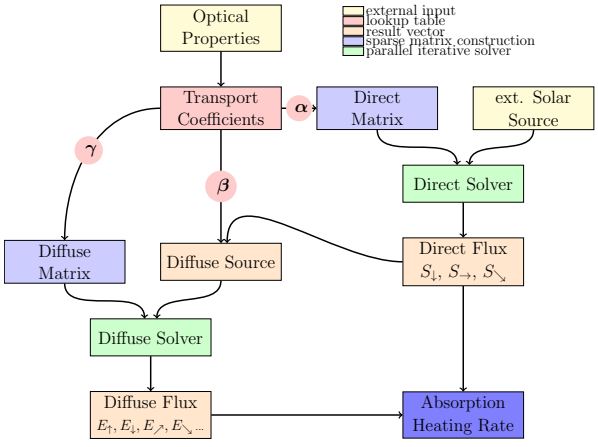

Figure 3: Flowchart for the conceptual steps of the solver. Input to the algorithm are optical properties and extraterrestrial incoming solar radiation. Output are the direct and diffuse fluxes as well as the absorption for each cell. Detailed description about the individual steps is given in section 2.5

one box equals the outgoing flux $E^B_\downarrow$ of the box above. The flux leaving one box to the right $E^R_\searrow$ enters the next box from the left $E^L_\searrow$. Substituting the expressions results in a set of coupled linear equations.

In order to solve this set of equations, one needs to know the boundary conditions. In the case of radiative transfer in the solar spectral region, this is the surface albedo and the extraterrestrial incoming radiation at top of atmosphere. In the one-dimensional case described for the TwoStream solver, the matrix can furthermore be written in a compact banded matrix with five diagonal entries, which can be solved efficiently with any numerical linear algebra package (e.g. LAPACK).

However, in the case of 3D solvers, it is generally not possible to order the matrix rows in a way that the matrix reduces to a low bandwidth, banded structure. Due to the horizontal coupling, the matrix is of size $N_{streams} \times N_{levels} \times N_x \times N_y$ where N_x and N_y are the numbers of grid boxes in the horizontal directions – a huge, yet sparse matrix (most entries are zero, see fig. 2).

Efficiently solving big sparse matrices on parallel machines is a demanding undertaking on its own. Numerous algorithms exist to solve such systems, but it is practically not possible to estimate in advance which method is suited best. This is where the parallel linear algebra library PETSc (Balay et al., 2014) comes into play. Using the PETSc Toolkit allowed a rapid development of the parallel algorithm and also allows the testing and comparison of a multitude of matrix solvers.

2.5. All the way to heating rates

With all the components in place, let us briefly summarize the outline of the RT model and the final steps to derive atmospheric heating rates. As shown in fig. 3, the input that needs to be provided externally are the optical properties of each grid box (absorption and scattering coefficient and asymmetry parameter) as well as the extraterrestrial solar source. It is clear from eq. (4) that direct radiation is not a function of the diffuse terms and can be solved prior to the diffuse radiation. In order to calculate the direct radiation we may set up the direct sub-matrix which consists only of α-coefficients. The α-coefficients are retrieved from the lookup table. Using the direct radiation together with β-coefficients, we set up the source term for the diffuse radiation. Assembling the dif-

fuse matrix and solving it results in diffuse fluxes. Using Gauss's theorem, we calculate the absorbed power dQ (divergence of radiation) inside each box by integrating the energy flux density over the surface of the box:

$$\frac{\mathrm{d}\boldsymbol{Q}}{\mathrm{d}t} = \iiint_V \boldsymbol{\nabla}\vec{E}\; dV = \oiint_S \vec{E}\cdot\vec{n}\; dS \tag{5}$$

In our case the energy flux through the box's surface is the sum of the net flux for all streams.

The heating rate is simply

$$\frac{\mathrm{d}\boldsymbol{T}}{\mathrm{d}t} = \frac{1}{c_p\rho}\cdot\frac{\mathrm{d}\boldsymbol{Q}}{\mathrm{d}t} \tag{6}$$

, where ρ is the air density and c_p the specific heat capacity.

3. Results and Discussion

In order to evaluate the results of the new solver, we compare the output to a full 3D Monte Carlo model, which serves as benchmark. MYSTIC (Monte Carlo code for the physically correct tracing of photons in cloudy atmospheres Mayer (2009)) has been developed as part of the radiative transfer library LibRadTran (Mayer et al., 2005). The code has been extensively validated in the Intercomparison of 3D Radiation Codes (I3RC, (Cahalan et al., 2005)). To compare the performance of the new solver with the widely used independent column approximation, we also calculated heating rates column by column for the given scenarios with a delta-eddington TwoStream solver, also included in LibRadTran.

As O'Hirok and Gautier (2005) noted, the ICA is expected to perform worst for vertically extended cloud fields at low sun angles. Radiative forcing is however suspected to be of most importance in shallow convective systems. For this reason we present results for both strongly and weakly forced situations and show that the algorithm performs well in both cases.

Details about the three cloud scenarios are given in table 2. Figures 4a to 4c show the respective vertically integrated optical depth. The '**Cb**'-scenario (fig. 4b) from the Goddard Cumulus Cloud Ensemble (Zinner et al., 2008) includes a cumulonimbus topped with an ice anvil and surrounded by smaller convective clouds. The '**I3RC**'-scenario (fig. 4a) is a cumulus field from experiment-7 of the Intercomparison of 3-Dimensional Radiation Codes (Cahalan et al., 2005). The '**astex**'-scenario (fig. 4c) is a stratocumulus cloud field (Albrecht et al., 1995) with a homogeneous stratus layer and sporadic convective cells.

	I3RC	**Cb**	**astex**
Δx,Δy (m)	70	250	40
min. Δz (m)	40	200	20
domain size (km^2)	6.7 x 6.7	64 x 64	10 x 10
cloud type	Cu	Cb	St
cloud phase	water	water&ice	water
cloud base (km)	1.0	3	2.4
cloud top (km)	2.4	16	2.5

Table 2: Details on cloud scenarios that were used to demonstrate algorithm performance. Each cloud scenario is described by the horizontal resolution Δx and Δy, the minimum vertical extent of a layer Δz (grid is stretched towards top of atmosphere), the total domain size, and cloud classifications. See fig. 4 for the horizontal distribution of clouds.

We compare the surface heating (direct irradiance $S_\downarrow$ plus net diffuse irradiance $E_\downarrow - E_\uparrow$) and atmospheric heating rates. The error is given by the relative root mean square error and the relative bias:

$$\begin{aligned} rel.\ \mathbf{RMSE} &= \frac{\sqrt{\overline{(y-x)^2}}}{\bar{x}}\cdot 100\% \\ \mathbf{bias} &= \left(\frac{\bar{y}}{\bar{x}} - 1\right)\cdot 100\% \end{aligned} \tag{7}$$

where y is either the IPA TwoStream calculation or the TenStream method. We treat the Monte Carlo result as truth and hence x stands for the 3D MYSTIC calculation and $\bar{x}$ for its arithmetic mean.

All calculations were performed using a constant surface albedo of 5 %. Integrated solar fluxes were calculated with the correlated-k method by Kato et al. (1999). We used 10^4 photons per pixel for the Monte Carlo calculations. The noise (standard deviation) of atmospheric heating rates is approximately 7 % in the case of **I3RC**, 4.5 % for **Cb** and 4 % for the **astex**-scenario. Likewise, for the surface heating, 3.6 %, 1.6 % and 4 %, respectively.

A qualitative look at fig. 5 visualizes the differences between the ICA TwoStream and TenStream solver. The slanted path of the direct radiation is clearly visible, which leads to strong heating at the cloud side, to elongated and displaced shadowing and generally higher heating rates in the atmosphere.

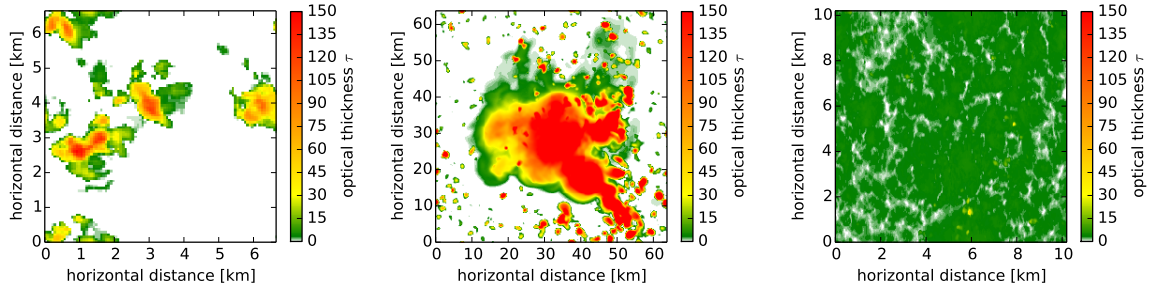

(a) **I3RC** (b) **Cb** (c) **astex**

Figure 4: Vertically integrated optical depth. Scattering and absorption optical depth spectrally integrated with correlated-k method of Kato et al. (1999). Optical depth truncated for fig. 4b ($\tau_{max} = 689$). Figure 4a depicts the scattered cumulus clouds with clear-sky regions in-between. Figure 4b shows the massive deep-convective cell, surrounded by small cumulus clouds. Lastly, fig. 4c shows the uniformly overcast stratus scenario.

		I3RC				**Cb**				**astex**			
	θ	TwostrICA		Tenstr		TwostrICA		Tenstr		TwostrICA		Tenstr	
Heating Rates in atmosphere	0	44	(-1.2)	16	(-0.8)	37	(-1.6)	20	(-2.1)	11	(-1.0)	8	(-0.6)
	20	60	(-3.0)	20	(-0.6)	58	(-3.1)	21	(-1.9)	14	(-1.4)	9	(-0.7)
	40	100	(-6.6)	23	(-0.6)	99	(-6.5)	23	(-1.8)	21	(-2.1)	12	(-0.4)
	60	171	(-12.2)	31	(-0.5)	158	(-11.9)	30	(-1.4)	40	(-1.1)	20	(2.0)
	80	376	(-16.2)	64	(1.5)	344	(-15.3)	62	(-0.1)	127	(0.2)	36	(3.2)
Surface Heating	0	20	(-2.3)	11	(-1.6)	24	(-4.3)	15	(-2.8)	10	(-0.6)	8	(-5.1)
	20	42	(-1.6)	14	(-1.7)	45	(-3.8)	15	(-2.9)	15	(-0.3)	9	(-4.7)
	40	55	(-0.1)	13	(-1.5)	66	(-2.5)	17	(-2.4)	15	(0.9)	9	(-3.0)
	60	62	(4.4)	17	(-1.1)	92	(1.1)	26	(-1.4)	16	(4.0)	11	(-0.2)
	80	65	(24.2)	44	(-0.1)	96	(27.6)	73	(-0.3)	18	(11.7)	8	(2.1)

Table 1: Relative RMSE and in parentheses the bias are given in percent for the surface heating (direct plus diffuse downward minus upward) as well as atmospheric heating rates. Two methods, namely a IPA delta eddington TwoStream and the new Tenstream solver are compared to calculations of the 3D MonteCarlo (MYSTIC) solver. Calculations for the three scenarios, **I3RC**, **Cb** and **astex** were performed for solar zenith angles $\theta = 0, 20, 40, 60, 80°$ and a constant surface albedo of 5 percent.

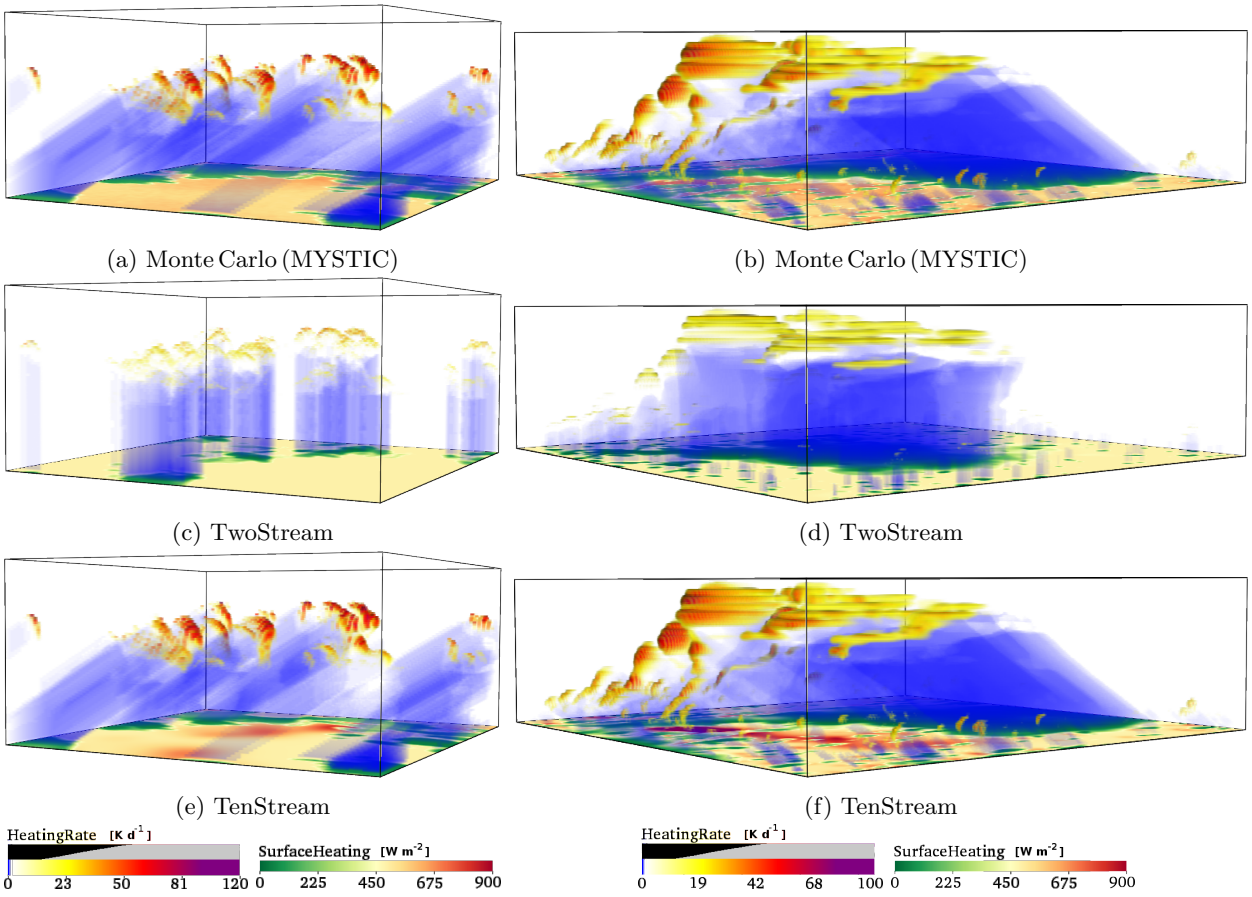

(a) Monte Carlo (MYSTIC) (b) Monte Carlo (MYSTIC)

(c) TwoStream (d) TwoStream

(e) TenStream (f) TenStream

Figure 5: Volume rendered perspective on atmospheric and surface heating rates (see section 3 for details). On the left side, scenario **I3RC** and on the right, scenario **Cb**. In the top row are benchmark 3D Monte Carlo MYSTIC calculations, in the mid row are delta-eddington TwoStream results and in the bottom row are TenStream calculations. Surface heating is solar net radiation in $\mathrm{W\,m^{-2}}$ and atmospheric heating rate given in $\mathrm{K\,d^{-1}}$. It is clear that the ICA TwoStream solver is not able reproduce the 3D RT effects, namely the cloud side illumination and the displacement of the shadows. In contrast, the TenStream solver realistically models the 3D effects. The only notable differences between the 3D MYSTIC calculations and the TenStream approximation are the local maxima in the surface heating. While the total surface heating is not biased (table 1), this suggests, that the TenStream is less "diffusive" than the benchmark Monte Carlo solver.

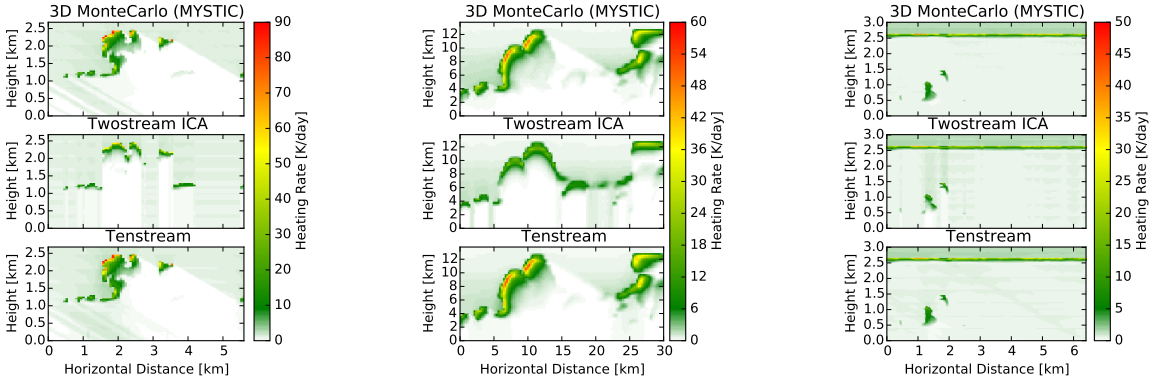

(a) **I3RC** (b) **Cb** (c) **astex**

Figure 6: Vertical cross-sections for heating rate profiles. Solar zenith angle $\theta = 60°$

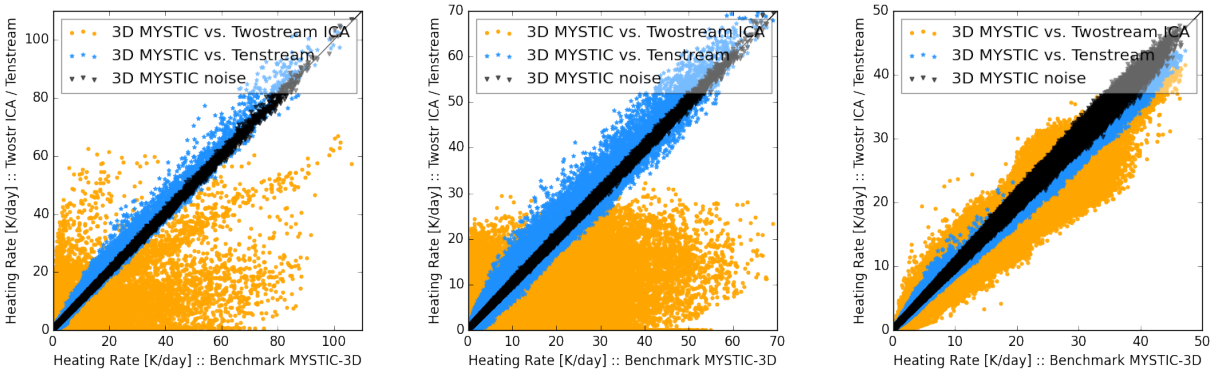

(a) **I3RC** (b) **Cb** (c) **astex**

Figure 7: Comparison of atmospheric heating rates to benchmark MYSTIC calculations. The black markers show the difference to an independent MYSTIC calculation with the same number of photons (Monte Carlo noise). The blue markers show the difference to the TenStream calculation and orange markers to an ICA TwoStream calculation. Solar zenith angle $\theta = 60°$. The TenStream solver is able to reproduce the higher heating rates and also at the correct position. Due to the horizontal homogeneity in the **astex** scenario the ICA is an adequate approximation.

Figure 6 shows a cross-section through the **I3RC**-scenario and allows a quantitative comparison between the solvers. Three dimensional RT calculations lead to higher heating rates at sunlit cloud sides than in ICA calculations. Figure 7a not only shows that the TenStream solver is able to produce the higher heating rates, but also that the spatial correlation is better than in the TwoStream case. Furthermore, the TenStream solver considerably reduces the RMSE for all scenarios independent of solar zenith angle (see table 1).

Regarding the surface heating, the performance of the algorithm deteriorates for large solar zenith angles. This is mainly caused by numerical diffusion. Figure 8 shows the difference in downwelling radiation between a Monte Carlo and a TenStream calculation. Note that numerical diffusion of direct radiation leads to a smoothing of the cloud shadow. Obviously, the longer the shadow *travels* through the atmosphere, the bigger the diffusion. A possible solution is to use more streams for the spatial discretization for the direct radiation. However, considering that numerical diffusion has the strongest impact for long "ray-paths" i.e. large solar zenith angles, we have to keep in mind that surface heating is weakest in these cases. We therefore think that the use of more streams is not required.

Computational speed. One important consideration is the computational speed of the new solver. The major part of the algorithm runtime is spent solving the sparse matrix equation. Big sparse matrices are

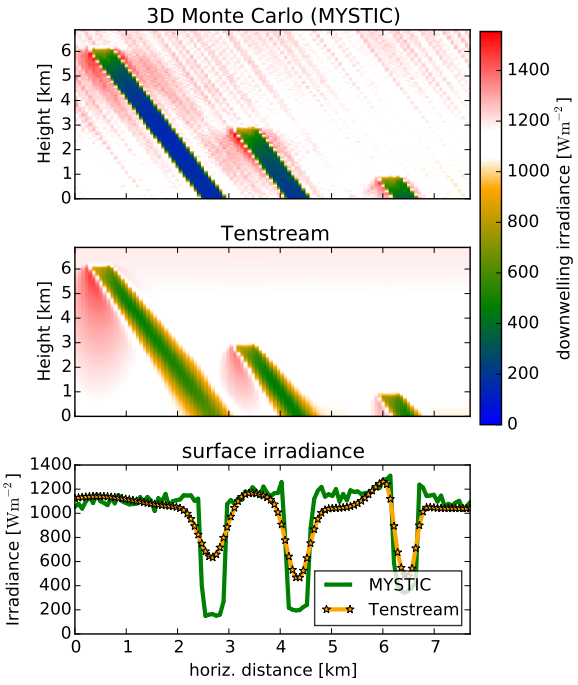

Figure 8: Downward radiation (direct plus diffuse downward) for three rectangular cubic clouds at different heights. 3D MonteCarlo (MYSTIC) calculation at top, Tenstream in the center, and below, the corresponding surface irradiance. Solar zenith angle $\theta = 20°$. Numerical diffusion in the TenStream solver results in smoothed shadows.

usually solved with iterative methods and the time needed to converge highly depends on the choice of matrix preconditioning and on which solver is used. The PETSc library allows the testing of a variety of different solvers, however such analysis is beyond the scope of this study and is therefore left for future research.

The matrix is positive definite and non-symmetric. For first test results, we used a stabilized bi-conjugate gradient iterative solver (BCGS) and an incomplete LU factorization preconditioning (Balay et al., 1997). Compared to the ICA TwoStream solver (using band-matrix LAPACK routines), the TenStream solver needed approximately 15 times longer. This value may decrease by using better matrix preconditioning and general code optimizations. One specifically interesting aspect in an atmospheric model is the reuse of the last solver call to supply the initial guess for the iterative solver which may significantly speed up the convergence. An increase by a factor of 15 for the radiative transfer calculations would typically increase the total runtime of an atmospheric model by roughly a factor of three. While this may prohibit the operational use on todays computers, it certainly allows for extensive experimental studies on cloud-radiation interactions. The TenStream solver presents a good approximation to the benchmark results, yet is orders of magnitude faster than Monte Carlo methods if the same accuracy is demanded.

4. Summary and Conclusions

We presented a methodology to extend the one dimensional TwoStream theory to N-streams in three dimensions. The use of Monte Carlo methods to derive the transport coefficients allows the development of radiative transfer codes for any grid geometries, which was a special concern in perspective to the irregular grid of the new ICON-Model (Dipankar et al., 2015). Surface flux and atmospheric heating rates were compared to ICA and full 3D Monte Carlo benchmark results. The algorithm outperforms the ICA solver in all of the studied scenarios.

The TenStream solver, compared to the ICA, considerably reduces the error. In the case of the solar zenith angle $\theta = 60°$ the RMSE of atmospheric heating rates is reduced from 171% to 31% for the **I3RC** scenario. Similarly, for the **Cb** scenario the error is reduced from 158% to 30%. The TenStream solver therefore furnishes a sound parametrization to drive high resolution models with realistic radiative heating rates.

Earlier studies, which used 3D Monte Carlo radiative transfer calculations to drive the model (OHirok et al., 2005; Petters, 2009) were limited because of the overwhelming computational complexity: computation times of full 3D RT models require three orders of magnitude more time than TwoStream solvers. In contrast, the TenStream solver yields realistic heating rates while increasing the computational cost by a factor of 15. We are confident, that the TenStream solver will enable us to rigorously study the impact of three-dimensional radiative transfer effects on cloud formation or precipitation. The code is available for download at `https://github.com/tenstream`.

Acknowledgements

This work was funded by the Federal Ministry of Transport, Building and Urban Development (BMVBS) through the German Weather Service (Extramurales Forschungsprojekt FKZ 8) and the Federal Ministry of Education and Research (BMBF) through the High Definition Clouds and Precipitation for Climate Prediction (HD(CP)2) project (FKZ: 01LK1208A). We thank Ann Kristin Naumann for providing us with the **astex** LES output.

References

Albrecht, B. A., Bretherton, C. S., Johnson, D., Scubert, W. H., Frisch, A. S., 1995. The atlantic stratocumulus transition experiment-astex. Bulletin of the American Meteorological Society 76 (6), 889–904.

Balay, S., Abhyankar, S., Adams, M. F., Brown, J., Brune, P., Buschelman, K., Eijkhout, V., Gropp, W. D., Kaushik, D., Knepley, M. G., McInnes, L. C., Rupp, K., Smith, B. F., Zhang, H., 2014. PETSc users manual. Tech. Rep. ANL-95/11 - Revision 3.5, Argonne National Laboratory.

Balay, S., Gropp, W. D., McInnes, L. C., Smith, B. F., 1997. Efficient management of parallelism in object oriented numerical software libraries. In: Arge, E., Bruaset, A. M., Langtangen, H. P. (Eds.), Modern Software Tools in Scientific Computing. Birkhäuser Press, pp. 163–202.

Cahalan, R. F., Oreopoulos, L., Marshak, A., Evans, K. F., Davis, A. B., Pincus, R., Yetzer, K. H., Mayer, B., Davies, R., Ackerman, T. P., et al., 2005. The i3rc: Bringing together the most advanced radiative transfer tools for cloudy atmospheres. Bulletin of the American Meteorological Society 86 (9).

Dipankar, A., Stevens, B., Heinze, R., Moseley, C., Zängl, G., Giorgetta, M. A., Brdar, S., 2015. A large eddy simulation version of icon (icosahedral nonhydrostatic): Model

description and validation. Journal of Advances in Modeling Earth Systems.

Evans, K. F., 1998. The spherical harmonics discrete ordinate method for three-dimensional atmospheric radiative transfer. Journal of the Atmospheric Sciences 55 (3), 429–446.

Frame, J. W., Petters, J. L., Markowski, P. M., Harrington, J. Y., 2009. An application of the tilted independent pixel approximation to cumulonimbus environments. Atmospheric Research 91 (1), 127–136.

Harrington, J. Y., Feingold, G., Cotton, W. R., 2000. Radiative impacts on the growth of a population of drops within simulated summertime arctic stratus. Journal of the atmospheric sciences 57 (5), 766–785.

Henyey, L., Greenstein, J., 1941. Diffuse radiation in the galaxy. Astrophys. Journal 93, 70–83.

Iwabuchi, H., 2006. Efficient monte carlo methods for radiative transfer modeling. Journal of the atmospheric sciences 63 (9), 2324–2339.

Kato, S., Ackerman, T. P., Mather, J. H., Clothiaux, E. E., 1999. The¡ i¿ k¡/i¿-distribution method and correlated-¡ i¿ k¡/i¿ approximation for a shortwave radiative transfer model. Journal of Quantitative Spectroscopy and Radiative Transfer 62 (1), 109–121.

Marquis, J., Harrington, J. Y., 2005. Radiative influences on drop and cloud condensation nuclei equilibrium in stratocumulus. Journal of Geophysical Research: Atmospheres (1984–2012) 110 (D10).

Mayer, B., , Kylling, A., 2005. Technical note: The libradtran software package for radiative transfer calculations-description and examples of use. Atmospheric Chemistry and Physics 5 (7), 1855–1877.

Mayer, B., 2009. Radiative transfer in the cloudy atmosphere. In: EPJ Web of Conferences. Vol. 1. EDP Sciences, pp. 75–99.

Meador, W., Weaver, W., 1980. Two-stream approximations to radiative transfer in planetary atmospheres: A unified description of existing methods and a new improvement. Journal of the atmospheric sciences 37 (3), 630–643.

O'Hirok, W., Gautier, C., 2005. The impact of model resolution on differences between independent column approximation and monte carlo estimates of shortwave surface irradiance and atmospheric heating rate. Journal of the atmospheric sciences 62 (8).

OHirok, W., Ricchiazzi, P., Gautier, C., 2005. Incorporation of 3d shortwave radiative effects within the weather research and forecasting model. In: 15th ARM science meeting proceedings. Daytona Beach, Florida. pp. 14–18.

Petters, J. L., 2009. The impact of radiative heating and cooling on marine stratocumulus dynamics.

Wapler, K., Mayer, B., 2008. A fast three-dimensional approximation for the calculation of surface irradiance in large-eddy simulation models. Journal of Applied Meteorology & Climatology 47 (12).

Wissmeier, U., Buras, R., Mayer, B., 2013. pantica: A fast 3d radiative transfer scheme to calculate surface solar irradiance for nwp and les models. Journal of Applied Meteorology & Climatology 52 (8).

Zinner, T., Marshak, A., Lang, S., Martins, J. V., Mayer, B., 2008. Remote sensing of cloud sides of deep convection: towards a three-dimensional retrieval of cloud particle size profiles. Atmospheric Chemistry and Physics 8 (16), 4741–4757.